

We are IntechOpen, the world's leading publisher of Open Access books Built by scientists, for scientists

6,900

Open access books available

186,000

International authors and editors

200M

Downloads

Our authors are among the

154

Countries delivered to

TOP 1%

most cited scientists

12.2%

Contributors from top 500 universities



WEB OF SCIENCE™

Selection of our books indexed in the Book Citation Index
in Web of Science™ Core Collection (BKCI)

Interested in publishing with us?
Contact book.department@intechopen.com

Numbers displayed above are based on latest data collected.
For more information visit www.intechopen.com



Epitaxial Silicon Solar Cells

Vasiliki Perraki

*Department of Electrical and Computer Engineering, University of Patras,
Greece*

1. Introduction

Commercial solar cells are made on crystalline silicon wafers typically 300 μm thick with a cost corresponding to a large fraction of their total cost. The potential to produce good quality layers (of about 50 μm thickness), in order to decrease the cost and improve in the same time the efficiency of cells, has entered to the photovoltaic cell manufacturer priorities. The wafers thickness has been significantly decreased from 400 μm to 200 μm , between 1990 and 2006 while the cell's surface has increased from 100 cm^2 to 240 cm^2 , and the modules efficiency from 10% to already 13 %, with the highest values above 17% (Photovoltaic Technology Platform; 2007). Advanced technology's solar cells have been fabricated on wafers of 140 μm thicknesses, resulting to efficiencies higher than 20% (Mason.N et al 2006). The cost associated to the substrate of a crystalline silicon solar cell represents about 50-55% on module level and is equally shared between the cost of base material, crystallization and sawing (Peter. K; et al 2008). The cost related to the Si base material can be reduced fabricating thinner cells, while the cost of crystallization and sawing is eliminated by depositing the Si directly on a low cost substrate, like metallurgical grade Si. The epitaxial thin- film solar cells represent an attractive alternative, among the different silicon thin film systems, with a broad thickness range of 1-100 μm (Duerinckh. F; et al 2005). Conversion efficiencies of 11.5-12 % have been achieved from epitaxial solar cells grown on Upgraded Metallurgical Grade Silicon (UMG Si) substrates with an active layer of 30 μm , and an efficient BSF (Hoeymissenet. J.V; al 2008). Epitaxial cells with the same active layers deposited on highly doped multi-crystalline Si substrates by Chemical Vapor Deposition and the front and back surfaces prepared by phosphorous diffusion as well as screen printing technique, have confirmed also efficiencies 12.3% (Nieuwenhuysen. K.V; 2006). Solar cells developed by a specific process for low cost substrates of UMG silicon have led to efficiencies of 12.8% (Sanchez-Friera. P; et al 2006). Better results have been achieved from cells with an emitter epitaxially grown by CVD, onto a base epitaxially grown (Nieuwenhuysen. K.V; et al 2008). The emitter creates a front surface field which leads to high open-circuit voltages (V_{oc}) resulting to cell efficiencies close to 15% by optimizing the doping profile and thickness of epitaxial layers and by including a light trapping mechanism.

This chapter first describes the manufacturing procedures of epitaxial silicon solar cells, starting from the construction of the base layer until the development of solar cells.

Then a one- dimensional (1D) (Perraki.V; 2010) and a three dimensional (3D) computer program (Kotsovos. K & Perraki.V; 2005), are presented, for the study of the n^+pp^+ type

epitaxial solar cells. These cells have been built on impure (low cost) polycrystalline p⁺ silicon substrates (Upgraded metallurgical grade UMG-Si), by a special step of thin pure Si deposition followed by conventional techniques to build a n⁺/p junction, contacts and antireflective coating (ARC). The software developed expresses the variations of photovoltaic parameters as a function of epilayer thickness and calculates for different values of structure parameters, the optimised cell's photovoltaic properties. According to the one dimensional (1D) model, the photocurrent density and efficiency are calculated as a function of epilayer thickness in cases of low and high recombination velocity values, as well as in cases of different doping concentration values (Perraki.V; 2010), and their optimum values are figured. The parameter chosen for the cell's optimisation is the epitaxial layer thickness, through variation of grain size and grain boundary recombination velocity, according to the three dimensional (3D) model (Kotsovos. K, & Perraki. V, 2005). Furthermore, a comparison among simulated 3D, 1D and corresponding experimental spectral response results under AM 1.5 illuminations, is presented.

2. Epitaxial silicon solar cell fabrication

The manufacturing sequence for epitaxial silicon (Si) solar cell can be divided in the following main steps: base/active layer formation, junction formation, antireflective coating (ARC) and metallization (front and back contacts), including the oxidation technology, and auxiliary technologies. A complete flow diagram for the realisation of n⁺pp⁺ type epitaxial solar cells is presented in Table 1.

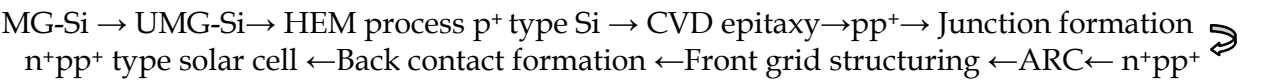


Table 1. Epitaxial solar cell's process

2.1 Base layer

The active layer of n⁺pp⁺ type crystalline Si solar cells is a thick layer doped with boron and is thus p-type layer with concentration of 10¹⁷ cm⁻³. The crystalline silicon photovoltaic technology has focused on reducing the specific consumption of the base material and increasing the efficiency of cells and modules and in the same time on using new and integrated concepts. Many research groups have tried to use very thin bases in silicon solar cells, aiming to decrease their cost. One of the possible ways for the achievement of cheap crystalline silicon solar cells on an industrial basis is the "metallurgical route". The different steps of this route are:
Metallurgical grade (MG), silicon powder (raw material) is upgraded by water washing, acid etching and melting, resulting to a material with insignificant properties and a measured value of diffusion length, L_n, smaller than 5 μm.
The Upgraded Metallurgical Grade (UMG), silicon is further purified and recrystallized into ingots by the Heat Exchange Method (HEM) so that to give crack-free ingots associated with large metal impurity segregation and cm size crystals, with better but still insignificant properties. This is due to the fact that the HEM technology allows removing metallic impurities, but the high concentration of boron, phosphorus and the presence of Si carbide precipitates are responsible for again very low measured values of L_n, and solar cell

efficiencies. In order to overcome the problem this material is used as a cheap p^+ -type substrate, on which a thin p-type epitaxial layer is formatted.

Epitaxial layer from pure Si is deposited, by chemical vapor deposition (CVD) on these impure UMG polycrystalline substrates, in an epitaxial reactor (Caymax.M, et al 1986). The wafers are first acid etched and cleaned at 1150 °C, then coated with silicon under SiH_2Cl_2 flow in H_2 gas at 1120 °C with a growth rate $1\mu m. min^{-1}$ (table 2). B_2H_6 is used, so that to get p- type layers. When the process has been completed a control is carried out testing the quality, thickness and dopant concentration. On to this layer the n^+/p junction is then built and epitaxial solar cells are realized, using a low cost screen printing technology.

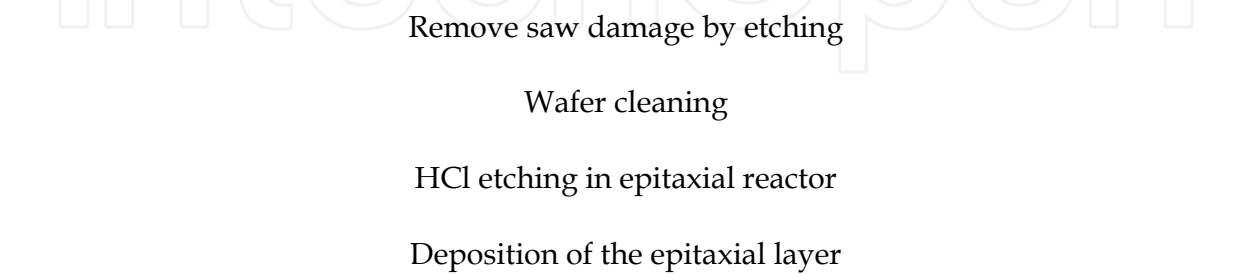


Table 2. Flow diagram of the CVD epitaxial process

The technology of Liquid Phase Epitaxy (LPE) has recently applied on metallurgical grade Si with interesting results as well (Peter.K et al 2002).

2.2 Junction formation

Two different approaches exist for the manufacture of the n^+ -p junction: the ion implantation and the diffusion from the solid phase or from the vapor phase (Overstraeten. R. J. V & Mertens. R, 1986).

- a. The ion implantation is characterized by excellent control of the impurity profile, low temperature processing, higher conversion efficiencies, and is rather used in the manufacture of spatial solar cells, due to the high costs associated with it.
- b. The diffusion process, from both gaseous and liquid phase, is usually applied for silicon solar cell fabrication. N_2 , Ar and O_2 are used as carrier gases, with quantities and mixing proportions as well as temperature, time and dopant concentration on the surface under, a very accurate control.

Diffusion from the vapor phase consists of diffusion of phosphorus from the oxide formed onto the silicon surface when N_2 carrier gas and $POCl_3$ are used in a heated open-tube furnace process at 800-900 °C. Disadvantages of the method are that, diffusion appears on both sides resulting to a back parasitic junction which has to be removed and non uniformity in cases of very shallow junctions.

Diffusion from a solid phase consists of deposition of a dopant layer at ambient temperature followed by a heat treatment, in an electrically heated tube furnace with a quartz tube, at a temperature ranging from 800 to 900 °C. This process can be performed using chemical vapor deposition (CVD), screen printing technique, spin-on or spray-on, forming thus only a junction on the front surface.

- i. The CVD technique concerns the deposition, at low temperature, of a uniform phosphorus oxide on the wafer’s front surface. This technique uses, highly pure, expensive, gases ensuring a uniform profile and defined surface conditions.

- ii. Screen printing is involved to thick film technologies which are characterized by low cost production, automation and reliability. In a first step, a paste rich in phosphorus is screen printed onto the silicon substrate. Then, phosphorus is diffused throughout a heat treatment in an open furnace, under typical peak temperatures between 900 and 950 °C, to form the n-p junction.
- iii. Spin-on and spray-on of doped layers yield to high throughput but non uniform surfaces.

2.2.1 Diffusion theory

As the diffusion procedure, is usually applied for silicon solar cell fabrication, it is necessary to refer in brief the theory of diffusion, of various solid elements in the Si solid. This process obeys to Fick's second law, which is expressed in one dimension by the following partial differential equation (Carslaw. H.S; and Jaeger .J.C 1959), (Goetzberger.A, et al 1998).

$$\frac{\partial N(\chi, t)}{\partial t} = D \frac{\partial^2 N(\chi, t)}{\partial \chi^2} \quad (1)$$

Where $N(\chi, t)$ stands for the concentration of the diffusing elements at point χ and time t and D the diffusion coefficient, characteristic of each material. This coefficient strongly depends on temperature according to the following relation (Sze. S. M. 1981).

$$D = D_0 \exp(-\Delta E / kT) \quad (2)$$

D_0 and ΔE (activation energy) are constant for a given element over wide temperature and concentration ranges.

The temperature plays a very important role in the diffusion process due to the temperature exponential dependency of diffusion coefficient. The diffusion coefficients in relation to temperature show that metals like Ti, Ag, Au, have higher diffusion coefficients D by several orders of magnitude compared to dopants As, P, B, and consequently they diffuse faster in Si, while elements such as Cu, Fe diffuse even more quickly. Therefore solar cell technology requires excellent cleanness of laboratory and experimental devices. However diffusion time does not affect so much the depth of penetration as this is proportional to its root square.

Two solutions to the partial differential equation 1 are considered. In the first case the dopant source is inexhaustible, the surface doping concentration N_s is considered constant during the diffusion process and the bulk concentration depends on diffusion time and diffusion temperature. The mathematical solution under boundary conditions concerning the parameters N_s , t , N_x , and χ reads:

$$N(\chi, t) = N_s \operatorname{erfc} \frac{\chi}{2\sqrt{Dt}} \quad (3)$$

Where, erfc stands for the complementary error function distribution.

In order to calculate the depth χ_j of the n-p junction, it is necessary to express the ratio of bulk concentration in the base silicon to surface concentration ($N_{\chi t} / N_s$) as a function of χ / \sqrt{Dt} and choose diffusion constant, temperature, and time.

In the second case, during the diffusion process there is an exhaustible dopant source on the surface with a concentration Q (cm^{-2}). The solution of the differential equation 1 $N(\chi, t)$ (Gaussian distribution) at point χ and time t is given by Eq 4:

$$N(\chi, t) = \frac{Q}{\sqrt{\pi Dt}} \exp\left(-\left(\frac{\chi}{2\sqrt{Dt}}\right)^2\right) \quad (4)$$

The surface concentration in this case is expressed as a function of the diffusion parameters by Eq 5:

$$N_s = \frac{Q}{\sqrt{\pi Dt}} \quad (5)$$

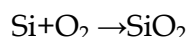
The penetration depth χ_j of the n-p junction is again calculated by the ratio of the concentration in the base silicon to surface concentration ($N_{\chi t} / N_s$) when diffusion constant, temperature and time are also determined.

2.2.2 Emitter's diffusion procedure

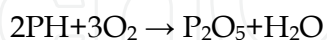
The silicon base wafers are etched, to remove damage from the wafering process (or to prepare after the CVD process) and cleaned, in order to introduce dopant impurities into the base in a controlled manner and form the n-p junction.

Since the starting wafers for solar cells are p-type, phosphorus is the n-type impurity generally used. The n⁺-doped emitter of the cell is thus created by the diffusion of phosphorus, in high concentration which is introduced in the form of phosphine (PH) or gaseous oxychloride (POCL₃) into the diffusion furnace. The later is introduced using nitrogen N₂, as a carrier gas. The disadvantages of this method are the formation of a back parasitic junction as the diffusion occurs on both sides and a non uniformity for very shallow junctions.

At the high temperatures of approximately 800 °C the dopant gases react with the surface of the silicon when oxygen is added, in accordance with the chemical reaction



Silicon dioxide (SiO₂) is produced on the surface and secondly, phosphine is converted to phosphorus pentoxide (P₂O₅) according to the following chemical reaction



The P₂O₅ created combines with the SiO₂ which is grown on the silicon surface to form liquid phosphorus silicate glass which becomes the diffusion source.

Phosphorus diffusion (at temperatures of 950 °C) as a function of diffusion time shows deviating behaviour from the theory for the case of low penetration depth. This behaviour has been explained by several authors; however it has the disadvantage for solar cells that a dead layer is created, of about 0.3 μm thickness, which reduces efficiency to approximately 10%. According to an advanced process, a dead layer can be impeded using a double diffusion process (Black. A. W, et al 1989). The first diffusion step consists of a predisposition coat with a low level diffusion of phosphorus at a temperature of approximately 800 °C. Then the phosphorus silicate glass layer is removed by chemical means and in a second diffusion step, this time at a temperature 1000-1100 °C, the desired

penetration depth of phosphorus is achieved. Surface concentrations of approximately 10^{19} cm^{-3} can be obtained.

2.2.3 Screen printing for junction formation

A process line based on the use of thick film technology offers advantages of low cost, automation, and reliability. The technology involves the screen printing technique for the junction formation. According to this a phosphorus-doped paste, containing active material, solvents and a thickener is printed through screens, onto a silicon substrate (Overstraeten. R. J 1986). After printing, the substrate is dried at 150°C allowing thus the solvents to evaporate. The phosphorus diffuses from the printed layer into the silicon during a heat treatment in a belt furnace in nitrogen under typical peak temperatures between 900 and 950°C . When screen printing is used for junction formation there is no parasitic junction formed at the back as in the case for open tube diffusion. However the layer that remains on the front of the cell after diffusion and the edges of the substrate which are doped due to contamination, have to be removed by etching in a proper chemical solution followed by a cleaning step.

Apart from the junction formation screen printing process can also be applied to the antireflection coating formation and the metallization (front and back contacts).

Epitaxial growth by CVD may also be used for the n^+ doped emitter formation, controlling the doping profile, on an epitaxially grown base. In this way a front surface field (FSF) is created yielding to a high open circuit voltage (V_{oc}) and high efficiency (Nieuwenhuysen. K.V; et al 2008).

2.3 Antireflection processes

2.3.1 Antireflection Coating (ARC)

Silicon surfaces reflect more than 33% of sunlight depending upon wavelength. For the manufacture of antireflection coatings industrial inks which contain titanium dioxide (TiO_2) or tantanium pentoxide (Ta_2O_5) as the active coating material, are used.

Two technologies are applied for this purpose:

- High vacuum evaporation technologies use almost exclusively TiO_2 , with a refraction index n adjusted between 1.9 and 2.3, a good transparency which favors high efficiencies and high costs.
- Thick film technologies, which are used in mass production due to their lower cost. At thick film technologies, a paste containing TiO_2 compounds is deposited onto the surface of silicon, either by the screen printing technique at temperatures of 600 to 800°C or by the spinning on technique.

The antireflective coating and the front side grid formation can be combined and made together by screen printing technique. In this case the TiO_2 paste is firstly dried at temperatures around 200°C , then a silver paste is added to it for the grid formation, and both are simultaneously sintered.

A further improvement can reduce total reflection to 3 – 4%. This can be achieved by using two antireflection layers, with a refractive index decreasing from the upper AR layer to the lower.

2.3.2 Textured surfaces

The textured surfaces of cells allow most of the light to be absorbed in the cell, after multiple reflections. For the construction of textured silicon surfaces the physical-chemical effect is

used, that the etching rate of silicon in an alkaline solution depends on the crystallographic orientation of silicon's front surface (Price J.B., 1983). The crystal orientation yielding to high efficiency solar cells is $\langle 100 \rangle$.

The anisotropic etching process takes place in weak solutions of KOH or NaOH with a concentration of 10% up to 30% at approximately 70 °C. This configuration results to inverted pyramid structures, under well determined conditions and reduces the reflection of sunlight to approximately 10 % (Goetzberger.A, et al 1998).

An additional ARC allows a further reduction to approximately 3%. In practice the best success has been achieved with inverted pyramids.

2.4 Contacts

2.4.1 The structuring of the finger grid

The technologies used for the structuring of the finger grid are three:

- a. The vacuum evaporation, which has the disadvantage that the smallest finger width is approximately 100 μm or at best 50 μm ,
- b. The photoresist technique which is used if narrower contact fingers are required in order to reduce shadowing.
- c. The screen printing technique, which uses metal pastes, and dominates in a wide range of production techniques as it is particularly cost effective, with the maximum finger width about 100 μm .

This technique is widespread in industrial solar cell manufacturing and has automating processes (Overstraeten. R.J.V; 1986). The screen printing process uses metal pastes containing in addition to 70% Ag approximately 2% sintered glass. After depositing, the layer is sintered at temperatures of about 600 °C, while the sintered glass components melt and dissolve a small layer of silicon. At the same time this melt is enriched by silver. Upon cooling a recrystallized Si layer is created as with normal alloying, which contains a high proportion of Ag and thus creates a good ohmic contact. This process gives quite low contact resistances on the n^+ emitter at surface concentrations of approximately 10^{20} cm^{-3} .

2.4.2 Back surface contacts

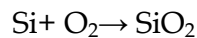
The realizations of back surface contacts need only aluminum, in the form of paste. This element has the advantage that forms alloys at its eutectic point 577 °C, and has a good solubility with concentrations of about 10^{19} cm^{-3} in Si, while a silver palladium paste is often sintered onto this layer in different cases (Overstraeten. R. J. V, & Mertens. R, 1986). Thus a high doping p^+ type is achieved in the recrystallised layer providing a Back Surface Field.

Normally sintering takes place at temperatures around 800 °C with the best results. A significant increase in V_{oc} is observed yielding thus higher values of solar cell efficiency.

2.5 Oxidation technologies

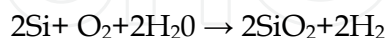
The oxidation technology is applied for the manufacture of a SiO_2 layer in solar cells. It is a relatively simple manufacturing process using high temperature treatment in an electrically heated tube furnace with a quartz tube under oxygen. This layer, nevertheless, plays a crucial role in silicon solar cells, with main characteristics passivation and masking effects of SiO_2 regarding impurities, which contributes positively to making silicon the basic material for most semiconductor devices.

Dry oxidation is achieved when silicon is heated without the addition of water vapour, and takes place according to the chemical reaction



As it is known, oxygen diffuses through the SiO_2 layer which is formed, there is no saturation thickness and the layer thickness grows in proportion to time or in proportion to the square root of time at greater layer thickness than $1\ \mu\text{m}$.

Wet oxidation, is achieved when silicon is exposed to water vapor, during the oxidation process and obeys to the following chemical reaction



Due to the hydrogen presence in case of wet oxidation the rate of growth is significantly higher than that of dry oxidation (Wolf H. F., 1976). Other influences that also alter the growth rate of SiO_2 are the doping concentration of silicon, the orientation of Si surfaces and the addition of chlorine ions during the oxidation process.

The use of SiO_2 as a passivating layer in solar cells has shown that dry oxidation under high oxidation temperatures yields very low surface recombination rates, which can be reduced even further by an annealing process at about 450°C , and depends upon the crystallographic orientation of silicon surfaces.

The masking effect of a SiO_2 layer in the diffusion process relies upon the fact that the diffusion rate of many diffusants in silicon dioxide is lower by orders of magnitude than in silicon itself. The required SiO_2 layer thickness, for different diffusion temperatures and times, shows that boron is masked by significantly thinner SiO_2 layers than is phosphorus. Furthermore, SiO_2 is used for masking in alkaline etching processes as well as for surface texturing (Goetzberger.A, et al 1998).

2.6 Back Surface Field (BSF)

The required p^+ doping in the starting wafer, in order to create a Back Surface Field, (BSF), is achieved by diffusion of boron. BBr_3 serves as the boron source for this purpose, which can be handled in a very similar manner to POCl_3 . As it is known, a BSF is necessary for high efficiency solar cells.

In industrial practice, aluminium with a eutectic point 577°C , is introduced onto the surface for the creation of a BSF. This is processed by vacuum evaporation or by screen printing technique at approximately 800°C .

2.7 Auxiliary technologies

Auxiliary processes such as etching and cleaning are necessary for the manufacture of solar cells.

Etching and cleaning techniques are used in order to make the surfaces of silicon wafers free of contaminants like molecular (residues of the lapping, polishing etc), ionic (from the etching solutions), or atomic (heavy metals). The most widely used procedure for surface cleaning is currently the RCA cleaning (named after the company RCA). This process is based upon the use of hydrogen peroxide (H_2O_2) firstly as an addition to a weak solution of ammonium hydroxide (NH_4OH) and secondly hydrochloric acid (HCl).

Etching of silicon dioxide layers occurs mainly in a weak solution of hydrofluoric acid, or in combination with ammonium fluoride (NH_4F).

Isotropic etching of silicon occurs in a solution of nitric acid and hydrofluoric acid or in combination with acetic acid and phosphoric acid (H_3PO_4).

Rinsing with deionised water must take place as the final stage, following all cleaning processes. With this processes, specific resistance values near to the theoretical value are achieved.

3. Mathematical model

A one dimensional (1D) analytical model is assessed via a simulation program which takes into account the interaction and the limitations between several parameters. By modeling short circuit current density J_{sc} , open circuit voltage V_{oc} and efficiency η , cells of different structure characteristics are studied. The photocurrent density and efficiency are estimated as a function of epilayer thickness d_2 , for various values of recombination velocity and doping concentration (Perraki V, 2010). Furthermore, the simulated and experimental plots of quantum efficiency are compared, under $1000\text{W}/\text{m}^2$ irradiation.

A three dimensional (3D) analytical model, which is based on the Green's Function method, is also implemented at the same cells. The model is applied via a simulation program to optimize the efficiency of cells. The parameter chosen for optimization is the epitaxial layer thickness via variation of grain size and grain boundary recombination velocity (Kotsovos K, & Perraki V., 2005). In addition, 3D spectral response data are compared with the 1D results.

3.1 One dimensional model

The epitaxial n^+pp^+ type Si solar cell is divided in four main regions (front layer n^+ , Space Charge Region (SCR), epilayer, and substrate), with thickness d_1-w_n , w_n+w_p , d_2-w_p and d_3 , respectively, figure 1.

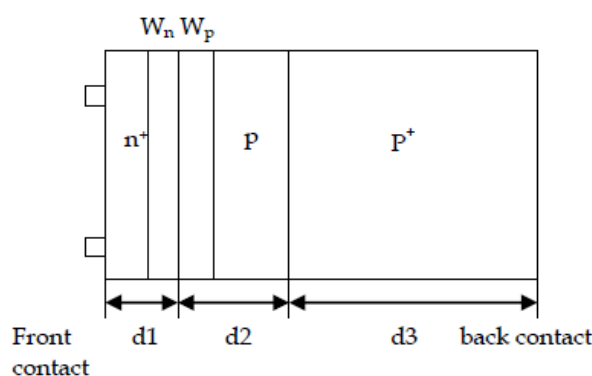


Fig. 1. The cross section for the theoretical model of n^+pp^+ type epitaxial solar cell.

There are a number of main assumptions used for modeling which concern, the homogeneity of physical and electrical properties of the grains (doping concentration, minority carrier mobility, life time and diffusion length). The grains are columnar, in Si materials recrystallized by the Heat Exchange Method, becoming increasingly large when considering successively, bottom, middle and top wafers in the ingot. These columnar grains are perpendicular to the front and to the n^+/p junction.

The front surface recombination velocity S_F has a value of 10^4 cm/s and the back surface S_B 10^{15} cm/s. A perfect abrupt interface between the heavily doped substrate with thickness higher

compared to its diffusion length and the lowly doped epilayer, consists a low/high junction p/p^+ . This junction produces a strong BSF while the p^+ layer does not contribute to the total photocurrent (Luque. A, & Hegeduw. S., 2003).

The expression, for the effective recombination velocity, S_{eff} , at the epilayer/substrate interface describing the quality of the back surface of the base, is given by the following equation (Godlewski. M; et al 1973):

$$S_{eff} = \frac{N_A D_{n^+}}{N_{A^+} L_{n^+}} \frac{\left(\frac{S_B L_{n^+}}{D_{n^+}} \cosh \frac{d_3}{L_{n^+}} + \sinh \frac{d_3}{L_{n^+}} \right)}{\left(\cosh \frac{d_3}{L_{n^+}} + \frac{S_B L_{n^+}}{D_{n^+}} \sinh \frac{d_3}{L_{n^+}} \right)} \quad (6)$$

Where, the terms N_A , N_{A^+} , L_{n^+} , D_{n^+} stand for the material's doping concentration, electron diffusion length and diffusion constant in the epilayer and the substrate respectively and S_B for the recombination velocity at the back surface. Due to the low/ high junction the following simplified relation (Arora. J, et al 1981) gives the expression for S_{eff} .

$$S_{eff} = \frac{N_A D_{n^+}}{N_{A^+} L_{n^+}} \quad (7)$$

The terms N_A , N_{A^+} , D_{n^+} and L_{n^+} are assumed constant all over of these regions' bulk.

The analytical form of the quantum efficiency of the front layer Q_p , is described by the following relation (Hovel H J 1975), (Sze. S. M, 1981):

$$Q_p = [1 - R] \frac{\alpha_n L_p}{(\alpha_n L_p)^2 - 1} \times \left[\frac{-\left(\frac{S_F L_p}{D_p} + \alpha_n L_p\right) + \left[\frac{S_F L_p}{D_p} \cosh \frac{d_1 - w_n}{L_p} + \sinh \frac{d_1 - w_n}{L_p}\right] \exp(-\alpha_n d_1 - \alpha_n w_n)}{\frac{S_F L_p}{D_p} \sinh \frac{d_1 - w_n}{L_p} + \cosh \frac{d_1 - w_n}{L_p}} + \alpha_n L_p \exp(-\alpha_n d_1 - \alpha_n w_n) \right] \quad (8)$$

Where L_p , D_p and α_n stand for hole diffusion length, diffusion coefficient and absorption coefficient in the front layer and R and S_F stand for reflection coefficient and front surface recombination velocity, respectively.

The base region quantum yield Q_n , can be calculated from the following relation

$$Q_n = [1 - R] \frac{\alpha_p L_n}{(\alpha_p L_n)^2 - 1} \exp(-(\alpha_n d_1 + \alpha_p W_p)) \left[\alpha_p L_n - \frac{\sinh \frac{d_2 - w_p}{L_n} + \frac{S_{eff} L_n}{D_n} \cosh \frac{d_2 - w_p}{L_n} + (\alpha_p L_n - \frac{S_{eff} L_n}{D_n}) \exp(-\alpha_p (d_2 - w_p))}{\frac{S_{eff} L_n}{D_n} \sinh \frac{d_2 - w_p}{L_n} + \cosh \frac{d_2 - w_p}{L_n}} \right] \quad (9)$$

α_p stands for the absorption coefficient in the base layer p.

The contribution of the space charge region Q_{SCR} is expressed by the following relation (Sze .S.M 1981)

$$Q_{SCR} = [1-R][\exp(-a_n W_n + a_p W_p) - 1] \exp(-a_n (d_1 - W_n)) \quad (10)$$

The contribution of the three regions of the solar cell is:

$$Q_{tot} = Q_p + Q_n + Q_{SCR} \quad (11)$$

The total photocurrent density J_{sc} arising from the minority carriers generated very near the junction in the n- layer, in the epilayer and in the space charge region can be calculated from the Eq. 12 as a function of the cell's quantum efficiency.

$$J_{SC} = q \int_{0.4}^{1.1} Q_{tot}(\lambda) N(\lambda) d\lambda \quad (12)$$

The flux of photons as a function of wavelength, $N(\lambda)$, was defined by a discretized AM1.5 solar spectrum.

The open circuit voltage depends on the Boltzmann constant, k , the solar cell operating temperate, T , the elementary electron charge, q , and the logarithm of the ratio between the photocurrent and dark current density, J_{sc} / J_0 .

$$V_{OC} = \frac{kT}{q} \ln\left(\frac{J_{SC}}{J_0} + 1\right) \quad (13)$$

Moreover, efficiency η (%) which is the most important parameter in the evaluation process of photovoltaic cells, is proportional to the open-circuit voltage V_{oc} , the photocurrent density J_{sc} , fill factor FF, and inversely proportional to the incident power of sunlight.

3.2 Three dimensional model (3D)

Several assessments have been admitted in order to simplify the 3D model and obtain the excess minority carrier density from the solution of the three-dimensional diffusion equation in each region.

The p/p⁺ junction is considered as a low/high junction, incorporating a strong BSF. It is assumed that the p⁺ region's contribution to the total photocurrent is negligible (Dugas.J, & Qualid. J, 1985).

The heat exchange method provides polycrystalline silicon with columnar grains, as shown in figure 2. The grain boundaries are surfaces of very small width compared to the grain size, characterized by a distribution of interface states. They are perpendicular to the n⁺/p junction, becoming increasingly large when considering successively, bottom, middle and top wafers in the ingot. Their physical and electrical properties, concerning the doping concentration, the mobility and diffusion length of minority carriers, along the three dimensions are homogeneous, for each region. There are ignored effects of other imperfections of the crystal structure.

The front and back surface recombination velocity S_F and S_B are the same as in (Luque. A, & Hegeduw. S., 2003), and their values are assumed as 10^4 cm/sec and 10^{15} cm/sec respectively. The effective grain boundary recombination velocity is assumed constant all over the surface of the grain and has been estimated to vary from 10^2 to 10^6 cm/sec. It

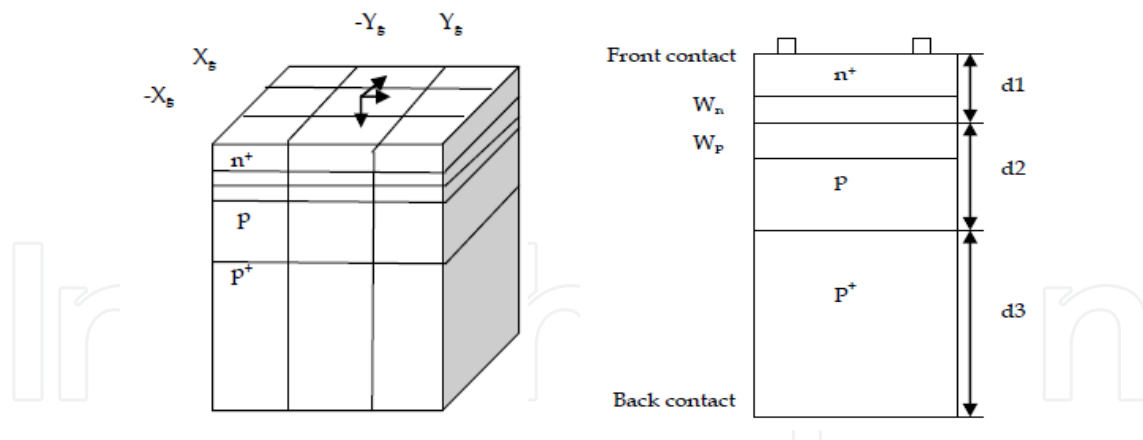


Fig. 2. Ideal crystal orientation and cross section for the theoretical model of n⁺pp⁺ type epitaxial solar cell (with columnar grains).

depends basically on the interface state density at the grain boundary and the doping concentration of the semiconductor material (Card. H.C, & Yang. E.,1977).

The solution of the three-dimensional diffusion equation provides the excess minority carrier density.

The steady state continuity equation for the top side of the junction under illumination is expressed by the following relation (Sze. S. M, 1981):

$$\nabla^2(p_n - p_{n0}) - \frac{p_n - p_{n0}}{L_p^2} = -\frac{\alpha(\lambda)F(\lambda)\exp(-\alpha(\lambda)z)}{D_p} \quad (14)$$

Where, $p_n - p_{n0}$, L_p and D_p stand for the excess minority carrier density in the front layer, the minority carrier diffusion length and the diffusion coefficient respectively. The material absorption coefficient $\alpha(\lambda)$ is given by Runyan (Runyan. W. R, (1976)) and the light generation rate F (number of photons of wavelength λ inserting the front side per unit area and unit time) is given by the following relation

$$F(\lambda) = N(0, \lambda)(1 - R(\lambda)) \quad (15)$$

With $N(0, \lambda)$ representing the number of photons of wavelength λ incident on the surface per unit area and unit time (depth $x=0$) and $R(\lambda)$ the reflection coefficient of light at the front side. This coefficient is calculated, for an antireflective coating of single layer (TiO_2) with optimal thickness 77 nm, (Heavens. O. S, 1991). There is a metal coverage coefficient of 13.1%, corresponding to the front metal grid and cell series resistance (R_s) of about 1.7 Ω .

The boundary conditions which accompany Eq. 14 when the solar cell is short circuited involve the front surface recombination velocity S_F and the grain boundary recombination velocity in the front region S_{pg} .

The diffusion equation for the base region is expressed by a similar form like in the front layer:

$$\nabla^2(n_p - n_{p0}) - \frac{n_p - n_{p0}}{L_n^2} = -\frac{\alpha(\lambda)F(\lambda)\exp(-\alpha(\lambda)z)}{D_n} \quad (16)$$

Where, $n_p - n_{p0}$ expresses the excess of electron concentration, L_n the corresponding diffusion length and D_n electron diffusion coefficient. The previous equation is subjected also to

specific boundary conditions when the device is operated under short circuit, concerning the grain boundary recombination velocity in the active layer S_{ng} and the effective back surface recombination velocity S_{eff} at the low / high junction. The simplified relation gives the expression for effective electron recombination velocity S_{eff} , as a function of the material's doping concentration of the active layer and the substrate (N_A , N_A^+), assumed constant all over of these regions' bulk (Eq.7). Moreover the grain boundary recombination velocity in the front and the active layer is considered the same and symbolized as S_{gb} .

The solution of the continuity equations (14) and (16) is obtained in analytical form using the Green's function method. This procedure is briefly described in (Kotsovos. K & Perraki. V; 2005). The analytical expression of the front layer photocurrent density J_p is derived, by differentiating the hole density distribution in the junction edge region $z=d_1-w_n$ presented in the form of infinite series (Halder. N.C, & Williams. T. R., 1983):

$$J_p(x, y, \lambda) = 4q\alpha F \times \sum_{m,n} \frac{L_{peff} M_x^2 N_y^2 \sin(mX_g) \sin(nY_g)}{mn(\alpha^2 L_{peff}^2 - 1)} \cos(mx) \cos(ny) \times \left[\frac{N_p + \alpha L_{peff} - \exp(-\alpha(d_1 - w_n)) \{N_p \cosh(\frac{d_1 - w_n}{L_{peff}}) + \sinh(\frac{d_1 - w_n}{L_{peff}})\}}{N_p \sinh(\frac{d_1 - w_n}{L_{peff}}) + \cosh(\frac{d_1 - w_n}{L_{peff}})} - \alpha L_{peff} \exp(-\alpha(d_1 - w_n)) \right] \quad (17)$$

where the variables x and y represent arbitrary points inside the grain and M_x , N_y , L_{peff} , N_p are expressed by proper equations as functions of S_{pg} , D_p , X_g , Y_g , L_p , and S_F .

In a similar way the analytical expression of the base region photocurrent density J_n is given, in the form of infinite series, by differentiating the electron density distribution in the junction edge region $z=d_2-w_p$ by the relation

$$J_n = 4q\alpha F e^{-\alpha(d_1 + w_p)} \times \sum_{k,l} \frac{L_{neff} K_x^2 L_y^2 \sin(kX_g) \sin(lY_g)}{kl(\alpha^2 L_{neff}^2 - 1)} \cos(kx) \cos(ly) \times \left[\alpha L_{neff} - \frac{N_n \{ \cosh(\frac{d_2 - w_p}{L_{neff}}) - e^{-\alpha(d_2 - w_p)} \} + \sinh(\frac{d_2 - w_p}{L_{neff}}) + \alpha L_{neff} e^{-\alpha(d_2 - w_p)}}{N_n \sinh(\frac{d_2 - w_p}{L_{neff}}) + \cosh(\frac{d_2 - w_p}{L_{neff}})} \right] \quad (18)$$

Where K_x , L_y , L_{neff} , N_n are expressed as functions of S_{eff} , S_{ng} , D_n , X_g , Y_g , L_n .

The photogenerated current in the Space Charge Region (equal to the number of photons absorbed), is derived by the 1D model (Sze. S. M, 1981):

$$J_{SCR} = qF e^{-\alpha(d_1 - w_n)} \{1 - e^{-\alpha(w_n + w_p)}\} \quad (19)$$

The total photocurrent is given from the sum of all current densities in each region considering as it has been early referred (Dugas. J.& Qualid. J, 1985) that the substrate contribution is negligible:

$$J_{sc} = J_p + J_n + J_{SCR} \quad (20)$$

A similar analysis might also carried out, for the determination of the dark saturation current (J_0) by solving the continuity equations, for both regions, (Halder. N. C, & Williams. T. R., 1983). The derived expression of J_0 is then used for the calculation of open circuit voltage from Eq 13.

4. Optimization

A computer program has been developed according to the mathematical analysis which implements the 1D model previously described (3.1) for the optimization of cells parameters. The values of reflection coefficient $R(\lambda)$ which depends on the wavelength λ and is related to the anti reflecting coating, as well as the photon flux $N(\lambda)$ defined by a discretized AM1.5 solar spectrum, are inserted in the program via the modelling procedure. The grid structure of the cell covering about 13.1% of the front surface and the Back Surface Field are inserted in a similar way. Material properties are considered as previously described, however the required data must be inserted by the user manually e.g., data concerning front layer and substrate (thickness, doping concentration), concentration of the front layer N_D , front surface recombination velocity S_F and effective recombination velocity S_{eff} , e.t.c. This data is then used as the starting point for the optimisation process. The program calculates the external quantum efficiency of the studied cells in a wavelength range from $0.4\mu\text{m}$ to $1.1\mu\text{m}$, under 1000 W/m^2 illumination (AM1.5 spectrum). The optimisation is carried out by introducing the lower and upper bounds of the epilayer thickness which are 40 and $100 \mu\text{m}$ respectively (Perraki. V & Giannakopoulos. A.; 2005). The simulation is then performed in batch mode with respect to the input data, controlling the input and output of the simulator at the same time.

After completion of this operation, results are interpreted and assessed by the output interface. The simulated short circuit current density is initially evaluated through numerical integration for the corresponding spectrum, while efficiency of the cells is investigated in the next step.

A 3D model is applied (3.2) to the same type of cells in order to optimize their epitaxial layer thickness, taking into account the structure parameters. The program computes the external quantum efficiency of the studied cells. It also provides, through numerical integration, results for the optimum photocurrent density and efficiency for various values of grain size and grain boundary recombination velocity.

A comparison between the 3D simulated and experimental results of photocurrent, and efficiency under AM1.5 irradiance is performed, as well as between the quantum efficiency curves calculated through 3D model and the corresponding 1D results of the studied cells.

5. Influence of structure parameters on cell's properties

The simulations for n^+pp^+ type epitaxial silicon solar cells, have been performed under AM 1.5 spectral conditions. The experimental values, of emitter (thickness d_1 , diffusion length L_P

and doping concentration N_D), and substrate (thickness d_3 , diffusion length L_n^+ and doping concentration N_A^+), assigned to the model parameters are shown in Table 3.

Cell	$d_1(\mu\text{m})$	$L_p(\mu\text{m})$	$N_D(\text{cm}^{-3})$	$d_3(\mu\text{m})$	$L_n^+(\mu\text{m})$	$N_A^+(\text{cm}^{-3})$
B2	0.4	1	1.5×10^{20}	300	13	2.9×10^{19}
T2	0.4	1	1.5×10^{20}	300	18	1.9×10^{19}

Table 3. Experimental values of emitter and substrate characteristics.

The experimental values of epilayer properties (thickness d_2 , base doping concentration N_A , diffusion length L_n) and the best results of measured photocurrent density J_{sc} , open circuit voltage V_{oc} and efficiency η for the cells under investigation are shown in table 4.

Cell	$d_2(\mu\text{m})$	$N_A(\text{cm}^{-3})$	$L_n(\mu\text{m})$	$J_{ph}(\text{mA}/\text{cm}^2)$	$V_{oc}(\text{V})$	$\eta(\%)$
B2	64	1.5×10^{16}	64	25.05	542	9.3
T2	64	1.5×10^{16}	71	26.17	558	10.12

Table 4. Experimental values of epilayer properties.

5.1 One dimensional model

The one dimensional model was utilized to perform simulations that indicate the dependency of cell’s photovoltaic properties on recombination velocity and doping level, for the cells (B2, from the bottom of the ingot) as well as for cells (T2, from the top of the ingot). Optimal photocurrent density and efficiency are calculated as a function of epilayer thickness for two different values of recombination velocity, and two different values of doping concentration.

5.1.1 Influence of recombination velocity

Figure 3 shows that the photocurrent density is little influenced (Hoeymissen,J. V; et al 2008) in cases of low recombination velocity (10^2 cm/sec). On the contrary photocurrent density is heavily affected by the epilayer thickness in case of high recombination velocity (10^6 cm/sec) and a value ~ 30 mA /cm² is achieved for epilayer thickness values much higher than 65 μm . The evaluation of these results shows that the epilayer thickness of 50 μm represents a second best value, in case of low recombination velocity. The gain, for thicker epilayers than this, is minor with an increment in J_{sc} of approximately ~ 0.05 mA /cm², when the epilayer thickness increases by steps of 5 μm .

The plots of the efficiency with respect to epilayer thickness for two different values of recombination velocity are illustrated in figure 4.

It is observed that the efficiency of the studied cells, calculated for recombination velocity values of 100 cm/sec saturates ($\eta \sim 13.8\%$) for epilayer thickness values higher than $\sim 65 \mu\text{m}$ where the gain is minimal. However for recombination velocity values of 2.5×10^6 cm/sec the efficiency is lower enough for thin epilayers and saturates for thickness values higher than 85 μm . Higher efficiencies are referred to cells with small grains, in comparison to those of large grains, because of the presence of fewer recombination centres. Annotating these results it is found that when the epilayer thickness of these cells decreases to values $\leq 50 \mu\text{m}$ the maximum theoretical efficiency decreases by a percentage of 0.03 % to 0.07 % for $S_{eff} = 100$ cm/sec. It is particularly recommended that a second best value of epilayer thickness equals to 50 μm , given that the gain for higher epilayer thickness values is of minor importance.

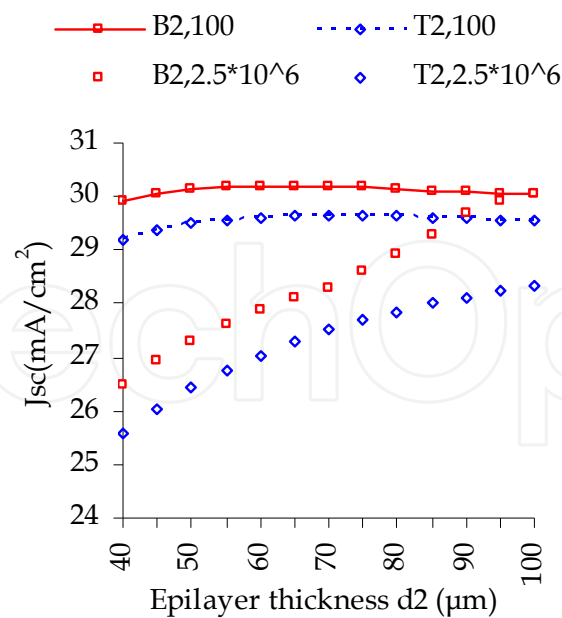


Fig. 3. Variation of short circuit current density, J_{sc} , of the studied cells (B2 with small grains, T2 with large grains) versus epilayer thickness d_2 , calculated for $S_{eff}=100$ cm/sec and 2.5×10^6 cm/sec.

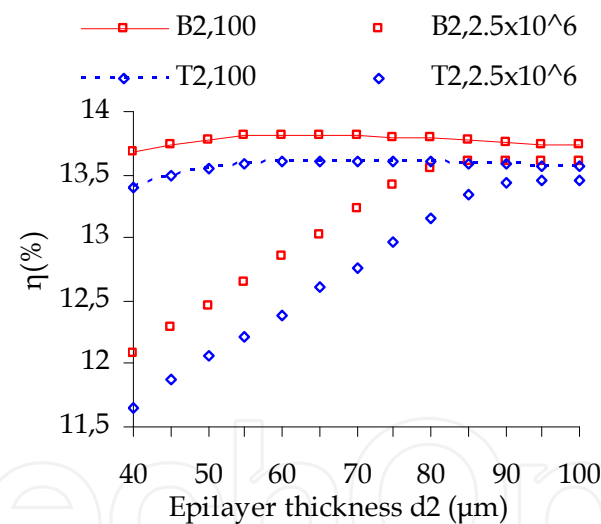


Fig. 4. Efficiency graph versus base thickness d_2 of the cells under investigation, calculated for $S_{eff} = 100$ cm/ sec and 2.5×10^6 cm/sec.

5.1.2 Influence of doping concentration

The same model was used to perform simulations indicating the relation between photovoltaic properties and doping concentration. When doping concentration increased from 10^{15} to 10^{17} cm^{-3} simulated data of the short circuit current density, J_{sc} , showed a small decrease, due to Auger recombination and minority charge carriers' mobility. Figure 5, illustrates the variation of J_{sc} with respect to epilayer thickness for two different values of doping. Maximum photocurrent densities are delivered from cells with epilayer thickness equal to 65 and 70 μm (B2 and T2 cells respectively). They vary between 29.6 and

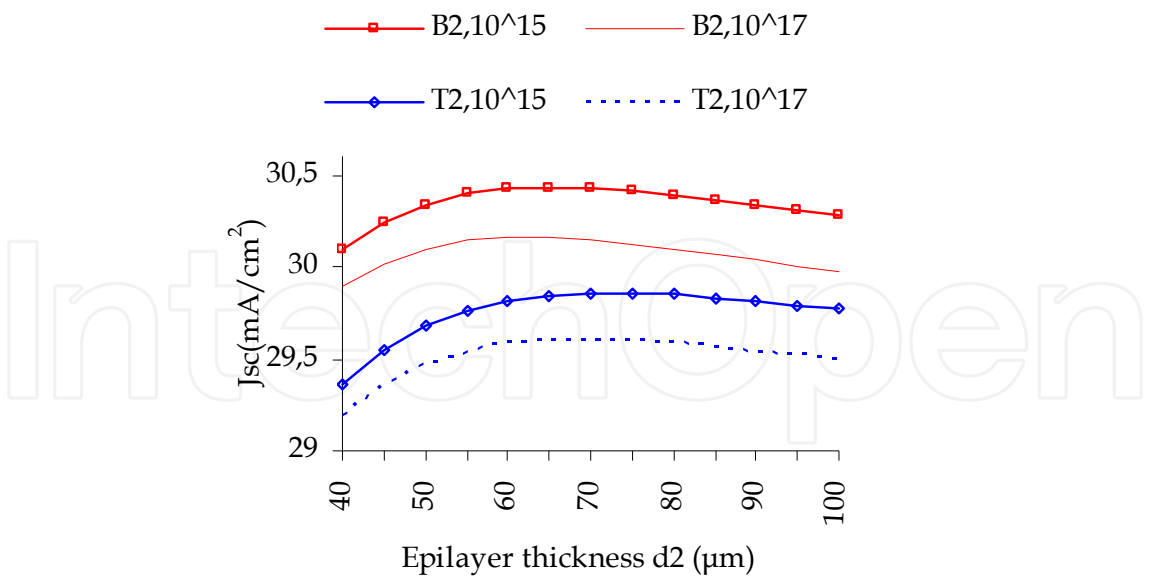


Fig. 5. Variation of the short circuit current density J_{sc} of the cells, as a function of base thickness d_2 calculated for doping concentration values of 10^{15}cm^{-3} , and 10^{17}cm^{-3} .

30.47 mA /cm², which are higher than experimental values. According to the calculated results when the epilayer thickness of B2 cells decreases to values $\leq 50\text{ }\mu\text{m}$, photocurrent density decreases for the different values of doping concentrations by approximately 0.05-0.08 mA/cm². It can be considered again that 50 μm , represent a second best value, since little is gained when the epitaxial layer becomes thicker.

Simulated data of cell efficiency, η , present a rise of its maximum value, as shown in figure 6, which is well above from maximum values experimentally obtained, and a shift of the optimum epilayer thickness to lower values. Higher efficiency has been calculated for cells with doping concentration of 10^{17}cm^{-3} compared to the one calculated for cells with doping

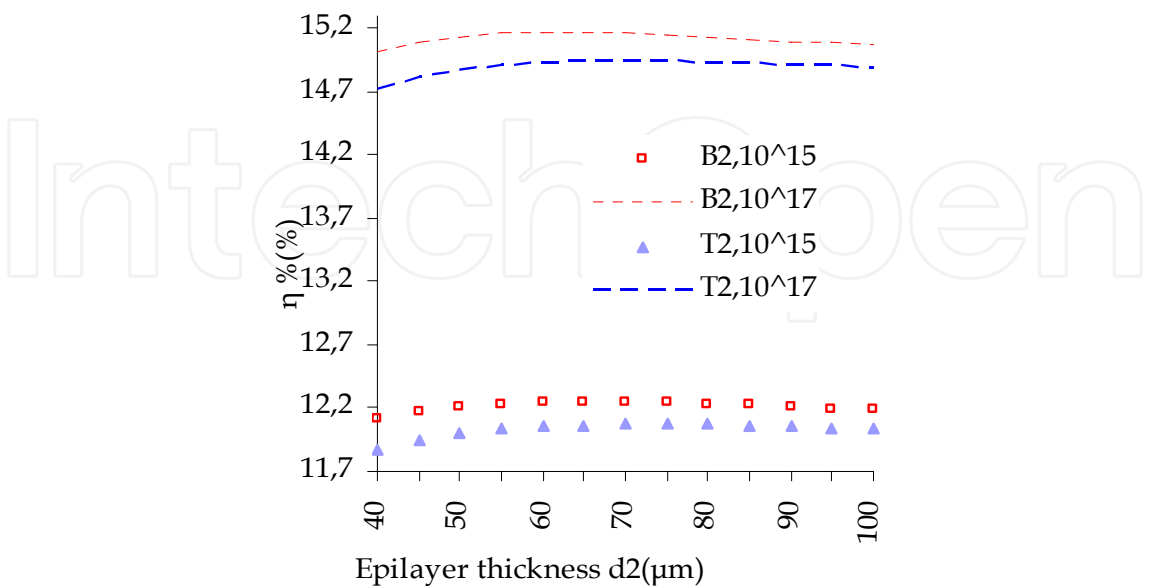


Fig. 6. Variation of the cell's efficiency as a function of epilayer thickness d_2 calculated for doping concentrations of 10^{15}cm^{-3} , and 10^{17}cm^{-3} .

of 10^{15} cm^{-3} . It is noticed that solar cell efficiency is insignificantly influenced by epilayer thickness variations. It is pointed that if the epilayer thickness of the small grain cell is reduced to values $\leq 50 \text{ } \mu\text{m}$, the efficiency decrease is less than 0.03%. Similarly a decrease in epilayer thickness, of T2 cells, to $50 \text{ } \mu\text{m}$ results in a decrease of their maximum efficiency by 0.04 %.

The optimized cell parameters J_{sc} and η for an optimum value of doping concentration show that even they are higher compared to the experimental ones, (Perraki. V.; 2010) they do not present significant differences for the two different types of cells. This is due to the fact that cell parameters introduced to the model were not very different and diffusion length values were high in all cases. It must be noted however that the optimum values of photocurrent density, efficiency and epilayer thickness calculated by this model are different than the ones corresponding to maximum J_{ph} and η and equal the values of saturation. When the epilayer thickness increases beyond the optimum value in steps of $5 \text{ } \mu\text{m}$, J_{sc} and η increase by a rate lower than 0.05 mA/cm^2 and 0.05% respectively. Taking all these into account, we can consider that the optimum value of efficiency is obtained for epilayer thickness values equal to or lower than $50 \text{ } \mu\text{m}$, which is much lower than base thickness and base diffusion length values of any solar cell.

The comparison between the experimental and the optimized quantum efficiency plots of B2 and T2 cells, (calculated by the 1D model) is presented in figure 7. The chosen model parameters, as shown in tables 3 and 4, provide a good fit to the measured QE data for wavelength values above $0.8 \text{ } \mu\text{m}$, whereas optimized curves indicate higher response for the lower part of the spectrum. The response of the experimental devices related to the contribution of the n^+ heavily doped front region (for low wavelengths of the solar radiation) is significantly lower than that of the simulated results, due to the non passivated surface.

Moreover, the spectral response of B2 is significantly higher compared to the one of T2 cell near the blue part of the solar spectrum, although cell T2 has higher experimental values of J_{sc} , V_{oc} and η . This may be explained by differences of the reflection coefficient between experimental and simulated devices and /or by the presence of fewer recombination centers in smaller inter-grain surfaces.

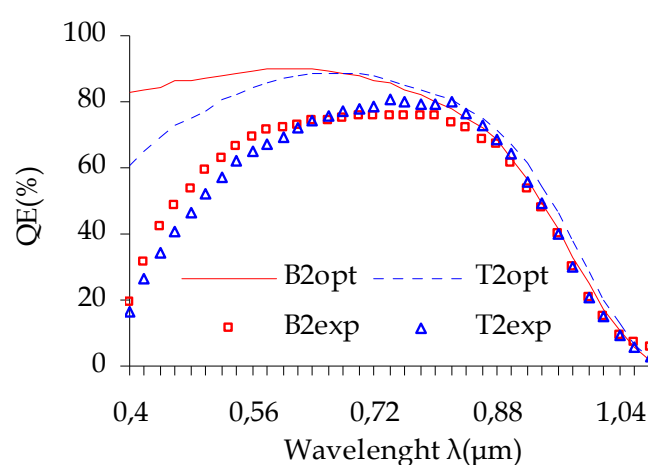


Fig. 7. Optimized external quantum efficiency for cells B2, and T2, evaluated for experimental values included in tables 3 and 4, and comparison with the experimental ones.

5.2 Three dimensional model

A 3D model was utilized to perform simulations that show the influence of grain boundary recombination velocity S_{gb} and grain size on cell's properties. The calculated results indicate the influence of grain boundary recombination velocity on the photocurrent and on the efficiency for various values of grain size for the cells B2 (from the bottom of the ingot) as well as for the cells T2 (from the top of the ingot). The plots are obtained for values of epilayer thickness maximizing the photocurrent which are not necessarily equal to the experimental. These optimal values of epilayer thickness used in the graph vary and depend on grain size and S_{gb} .

The graph of optimal photocurrent as a function of recombination velocity shows, figure 8, that it is seriously affected by recombinations in the grain boundaries of small grains, given that a significant amount of the photogenerated carriers recombine in the grain boundaries when grain's size is lower or comparable to the base diffusion length.

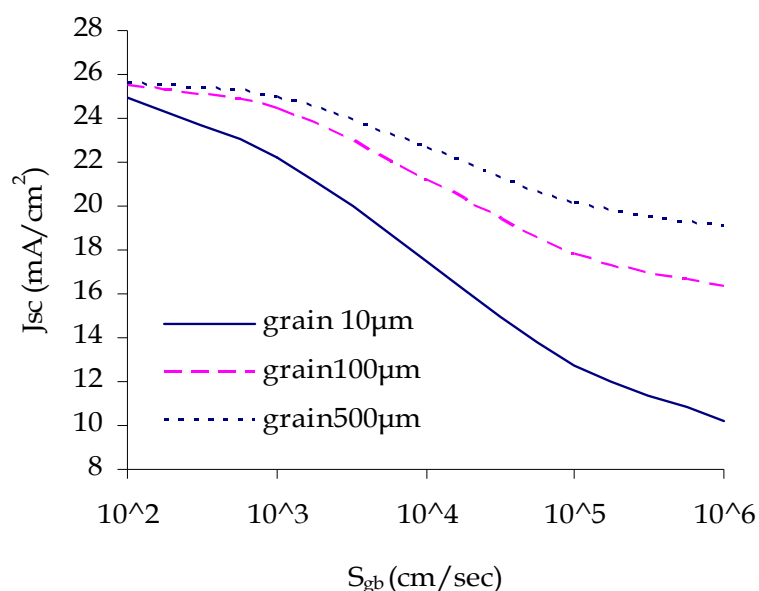


Fig. 8. Optimal short circuit current dependence on grain boundary recombination velocity S_{gb} of the cell B2, with grain size as parameter.

It is shown that the photocurrent density falls rapidly for grains with size 10 μm and high values of grain boundary recombination velocities. However, the effect of grain boundary recombination velocity is not so important for larger grain sizes (100 and 500 μm).

Figure 9 demonstrates the efficiency of the cells B2 in relation with the grain boundary recombination velocity for different grain sizes, which is calculated for optimal base thickness. It can be pointed that for small grain size, the efficiency is largely affected by grain boundary recombination, with a rapid decrease for recombination velocities greater than 10^3 cm/sec.

For larger grain sizes (500 μm), there is not so strong decrease with the recombination velocity, while insignificant decrease is observed in the efficiency for values lower than 10^3 cm/sec.

The graphs of optimal photocurrent as a function of grain boundary recombination velocity (figure 10) show that it is less affected from recombination in the grain boundaries for large grain sizes (cells T2), compared to cells with small grain sizes, (cells B2 in figure 8).

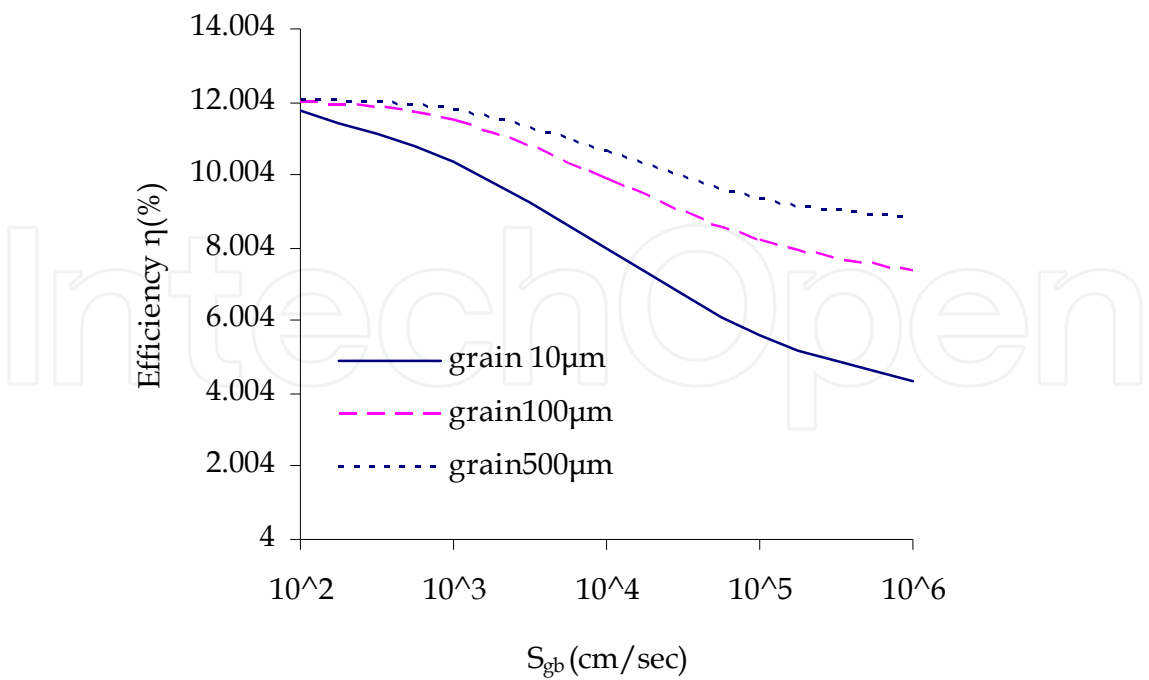


Fig. 9. Variation of efficiency η of the cell B2, as a function of grain boundary recombination velocity S_{gb} , calculated for optimal base thickness and variable grain sizes.

Therefore, for grains with size 5000 μm , and high values of grain boundary recombination velocities the photocurrent does not fall rapidly. It is evident that, for cells with even larger grain sizes (10000 μm) the influence of grain boundary recombination velocity is even more insignificant.

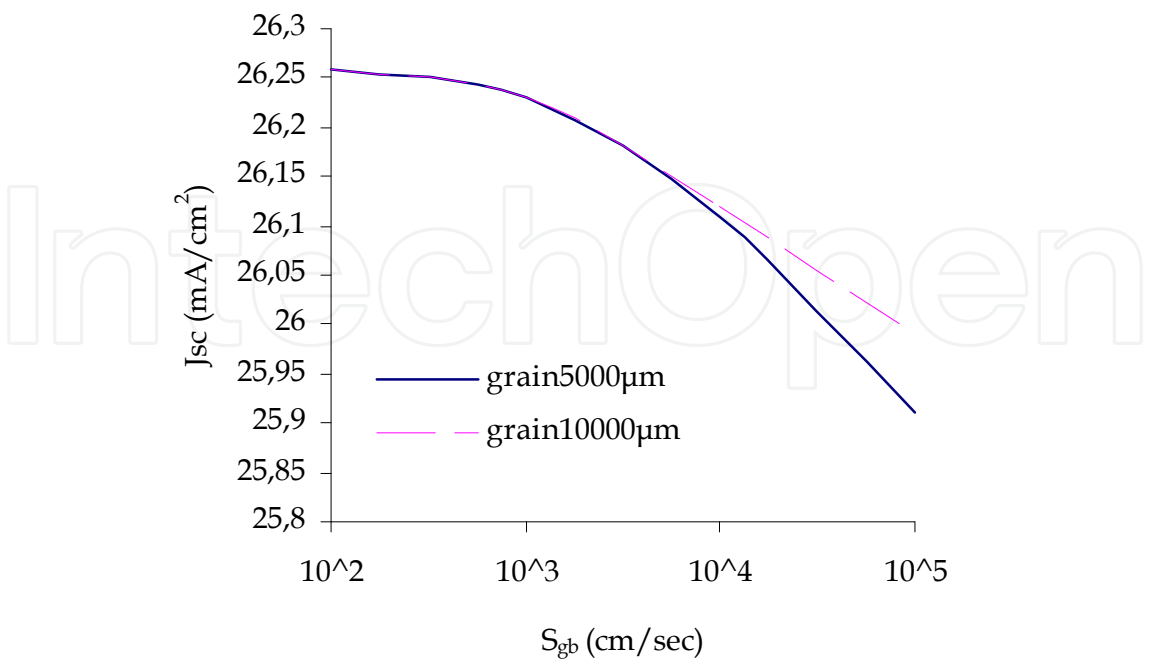


Fig. 10. Optimal short circuit current dependence on grain boundary recombination velocity S_{gb} of the cell T2, with grain size as parameter.

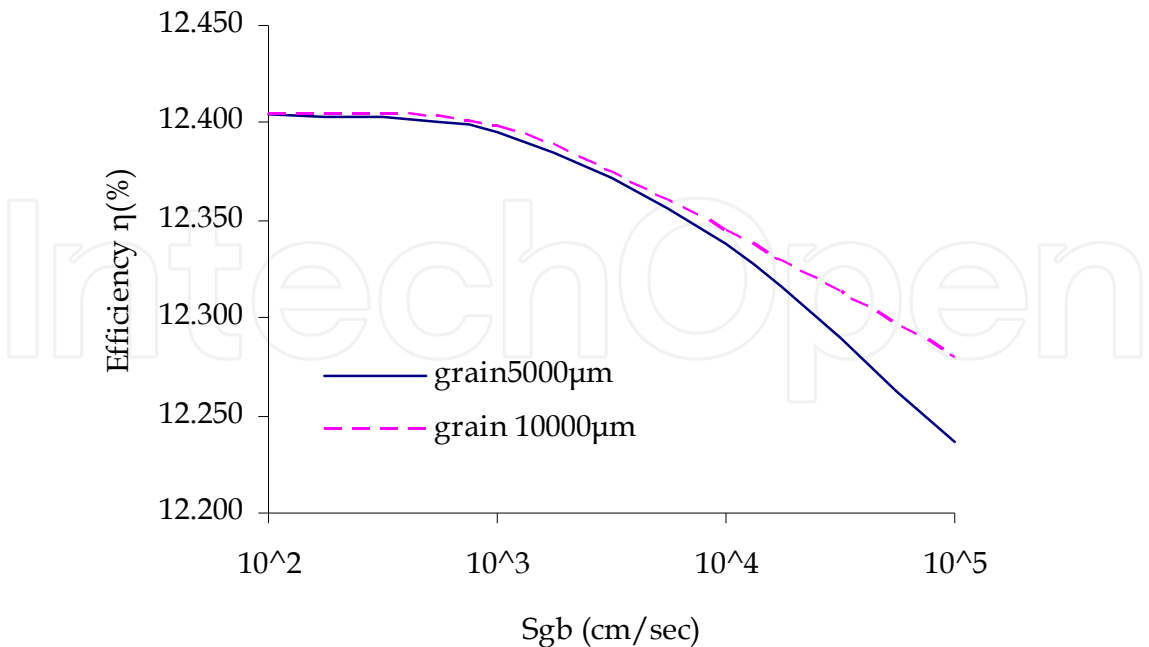


Fig. 11. Variation of the efficiency η as a function of grain boundary recombination velocity S_{gb} , calculated for optimal base thickness and variable grain sizes (cell T2).

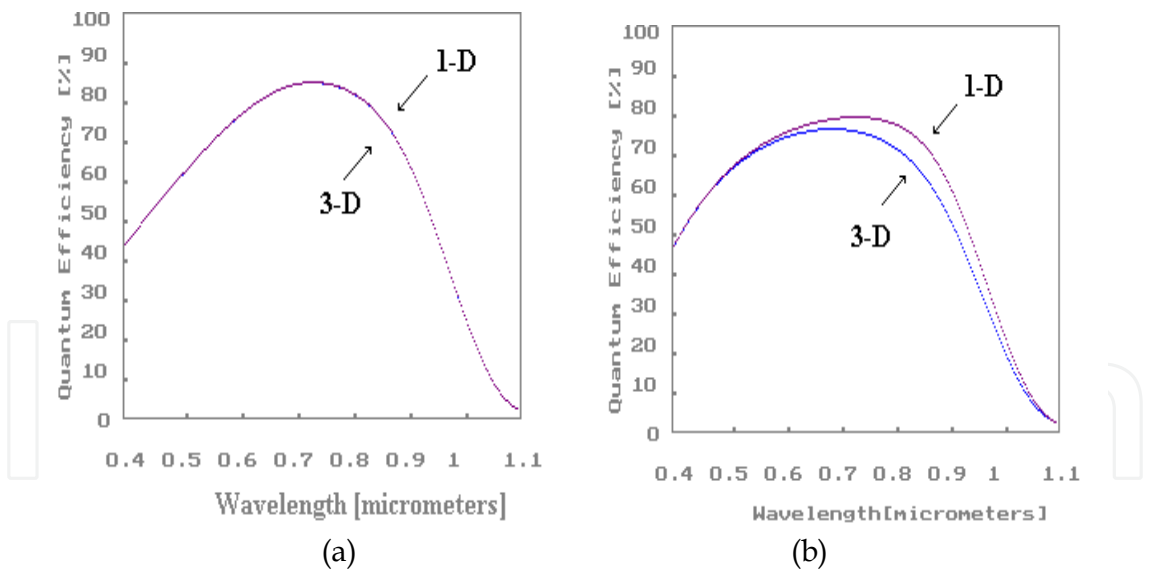


Fig. 12. Optimized external quantum efficiency and comparison with 3D model, for the cells B2 (a) and T2 (b), evaluated for experimental values included in tables 3 and 4.

Figure 11 illustrates the efficiency of the cells T2 as a function of grain boundary recombination velocity for different grain sizes, which is calculated for optimal base thickness. It can be observed that for large grain size, (5000 μm) the efficiency is less affected for grain boundary recombination for S_{gb} values higher than 10^3 cm/sec, compared to the case of small grain size, Fig. 9. A smoother decrease is observed in case of cells with even

larger grain sizes (10000 μm). It is obvious that solar cell efficiency saturates if S_{gb} is lower than 10^3 cm/sec and the gain is minimal for smaller values of grain boundary recombination velocity. In this case, efficiency is limited from bulk recombination, which is directly related to the base effective diffusion length L_n . However when grain boundary recombination velocity is reduced, the optimal layer thickness increases, until it reaches a value close to the device diffusion length L_n . This parameter seems to affect the value of optimal epilayer thickness. For higher S_{gb} values the maximum efficiency shifts to thickness values lower than the base diffusion length. However, for very elevated values of grain boundary recombination velocities and small grain size, the optimal thickness saturates to a value, which is the same for cells with thin or thick epilayer. The plots of L_{neff} and optimal epilayer thickness as a function of S_{gb} , show similar dependence on S_{gb} and grain size, with almost equal values (Kotsovos. K & Perraki.V, 2005).

The optimized 1D external quantum efficiency and the 3D graphs are demonstrated for the cells B2 and T2 in figure 12a and b respectively (Kotsovos. K, 1996). Since the influence of grain boundaries has not been taken into account in the 1D model it has shown superior response compared to the 3D equivalent for wavelength values higher than 0.6 μm (cell T2). Lower values of spectral response are observed in case of large grains (cell T2) and $\lambda > 0.6$ μm , possible due to the presence of more recombination centers in larger intergrain surfaces. However, very good accordance is observed between 1D and 3D plots for cells B2.

6. Conclusions

The optimal photocurrent and conversion efficiency for epitaxial solar cells are influenced by the recombination velocity. The best values of epilayer thickness and the effective base diffusion length are higher for lower values of grain boundary recombination velocities, resulting to higher efficiency values.

The comparison between the simulated 1D and experimental QE curves indicates concurrence for wavelengths greater than 0.8 μm . However, the measured spectral response close to the blue part of the spectrum was considerable lower compared to simulation data. On the other hand the comparison of the simulated 1D and 3D QE curves shows good agreement only for wavelengths lower than 0.6 μm for cells T2 and very good agreement for cells B2.

7. References

- Arora. J, Singh. S, and Mathur. P., (1981), *Solid State Electronics*, 24 (1981), p.739-747.
- Blackier. A. W, et al (1989) *Proc. 9th EUPVSEC*, Freiburg, Germany, p.328.
- Card. H.C, and Yang. E., (1977), *IEEE Trans. Electron Devices*, 29 (1977) 397.
- Carslaw. H.S; and Jaeger .J.C; 1959; *Conduction Heat in Solids*, 2nd ed, Oxford University Press, London 1959.
- Caymax. M; Perraki. V; Pastol.J. L; Bourée. J.E; Eycmans. M; Mertens. R; Revel. G; Rodot. M; (1986) "resent results on epitaxial solar cells made from metallurgical grade Si" *Proc.2nd Int.PVSE Conf* (Beijing1986)171.

- Duerinckh. F; Nieuwenhuysen. K.V; Kim. H; Kuzma-Filipek. I; Dekkers. H; Beaucarne. G; and Poortmans. J; (2005) "Large -area Epitaxial Silicon Solar Cells Based on Industrial Screen-printing Processes" *Progress in Photovoltaics* 2005,pp673
- Dugas.J, and Qualid. J, (1985), "3d modelling of grain size and doping concentration influence on polycrystalline silicon solar cells", *6th ECPVSEC*, (1985) p. 79.
- Godlewski. M; Baraona.C.R and Brandhorst.H.W 1973, *Proc 10th IEEE PV Specialist Conf.* (1973) P.40
- Goetzberger.A, Knobloch. J, Voss. B; *Crystalline Silicon Solar Cells*, John willey & Sons 1998.
- Halder. N.C, and Williams. T. R., (1983); "Grain Boundary Effects in Polycrystalline Silicon Solar Cells", *Solar Cells* 8 (1983) 201.
- Heavens. O. S, (1991); *The Optical Properties of Thin solid Films*, Dover, 1991.
- Hoeymissen. J.Van; Kuzma-Filipek. I; Nieuwenhuysen. K. Van; Duerinckh. F; Beaucarne. G; J. Poortmans. J; (2008) "Thin-film epitaxial solar cells on low cost Si substrates: closing the efficiency gap with bulk Si cells using advanced photonic structures and emitters", *Proceedings 23rd EUPVSEC* 2008 pp 2037.
- Hovel. H. J. (1975) *Solar cells Semiconductors and Semimetals* vol. II (New York: Academic
- Kotsovos. K; 1996, *Final year student Thesis*, University of Patras,Greece,1996
- Kotsovos. K and Perraki.V; (2005) "Structure optimisation according to a 3D model applied on epitaxial silicon solar cells :A comparative study" *Solar Energy Materials and Solar Cells* 89 (2005) 113-127.
- Luque. A, Hegeduw. S.,(ed) *"Handbook photovoltaic Science and Engineering "* Wiley, 2003.
- Mason. N; Schultz. O; Russel. R; Glunz. S.W; Warta. W; (2006) "20.1% Efficient Large Area Cell on 140 micron thin silicon wafer", *Proc. 21st EUPVSEC*, Dresden 2006, pp 521
- Nieuwenhuysen. K. Van; Duerinckh. F; Kuzma. I; Gestel. D.V; Beaucarne. G; Poortmans. J; (2006) " Progress in epitaxial deposition on low-cost substrates for thin- film crystalline silicon solar cells at IMEC" *Journal of Crystal Growth* (2006) pp 438..
- Nieuwenhuysen. K.Van; Duerinckx. K; Kuzma. F; Payo. I; Beaucarne. M.R; Poortmans. G; (2008); Epitaxially grown emitters for thin film crystalline silicon solar cells *Thin Solid Film*, 517, (2008) pp 383-384.
- Overstraeten. R.J.V, Mertens. R, (1986), *Physics Technology and Use of Photovoltaics*, Adam Hilger Ltd 1986.
- Perraki. V and Giannakopoulos.A; (2005); Numerical simulation and optimization of epitaxial solar cells; *Proceedings 20th EPVSEC* Barcelona 2005, pp1279.
- Perraki.V; (2010) "Modeling of recombination velocity and doping influence in epitaxial silicon solar cells" *Solar Energy Materials & Solar Cells* 94 (2010) 1597-1603.
- Peter.K; Kopecer.R; Fath. P; Bucher. E; Zahedi. C; *Sol. Energy Mat. Sol. Cells* 74 (2002) pp 219.
- Peter. K; R.Kopecek. R; Soiland. A; Enebakk. E; (2008) "Future potential for SOG-Si Feedstock from the metallurgical process route" *Proc.23rd EUPVSEC* (2008) pp 947
- Photovoltaic Technology Platform; (2007) "A Strategic Research Agenda for PV Energy Technology"; *European Communities*, 2007
- Price J.B., *Semiconductor Silicon*, Princeton, NJ, 1983, p. 339
- Runyan. W. R, (1976) *Southeastern Methodist University Report* 83 -13 (1976).

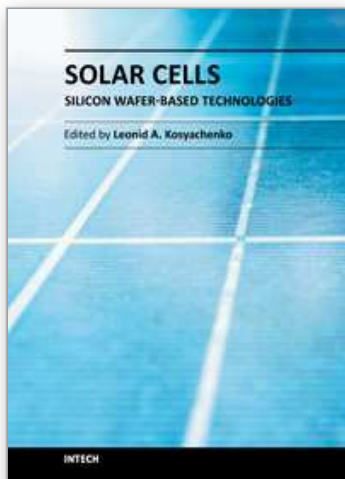
Sanchez-Friera. P; et al; (2006) "Epitaxial Solar Cells Over Upgraded Metallurgical Silicon Substrates: The Epimetsi Project" *IEEE 4th World Conference on Photovoltaic Energy Conversion*, pp1548-1551.

Sze. S. M; *Physics of Semiconductor Devices*, 2nd Ed, 1981, p 802

Wolf H. F., *Silicon Semiconductor Data*, Pergamon Press, 1976.

IntechOpen

IntechOpen



Solar Cells - Silicon Wafer-Based Technologies

Edited by Prof. Leonid A. Kosyachenko

ISBN 978-953-307-747-5

Hard cover, 364 pages

Publisher InTech

Published online 02, November, 2011

Published in print edition November, 2011

The third book of four-volume edition of 'Solar Cells' is devoted to solar cells based on silicon wafers, i.e., the main material used in today's photovoltaics. The volume includes the chapters that present new results of research aimed to improve efficiency, to reduce consumption of materials and to lower cost of wafer-based silicon solar cells as well as new methods of research and testing of the devices. Light trapping design in c-Si and mc-Si solar cells, solar-energy conversion as a function of the geometric-concentration factor, design criteria for spacecraft solar arrays are considered in several chapters. A system for the micrometric characterization of solar cells, for identifying the electrical parameters of PV solar generators, a new model for extracting the physical parameters of solar cells, LBIC method for characterization of solar cells, non-idealities in the I-V characteristic of the PV generators are discussed in other chapters of the volume.

How to reference

In order to correctly reference this scholarly work, feel free to copy and paste the following:

Vasiliki Perraki (2011). Epitaxial Silicon Solar Cells, Solar Cells - Silicon Wafer-Based Technologies, Prof. Leonid A. Kosyachenko (Ed.), ISBN: 978-953-307-747-5, InTech, Available from:
<http://www.intechopen.com/books/solar-cells-silicon-wafer-based-technologies/epitaxial-silicon-solar-cells>

INTECH
open science | open minds

InTech Europe

University Campus STeP Ri
Slavka Krautzeka 83/A
51000 Rijeka, Croatia
Phone: +385 (51) 770 447
Fax: +385 (51) 686 166
www.intechopen.com

InTech China

Unit 405, Office Block, Hotel Equatorial Shanghai
No.65, Yan An Road (West), Shanghai, 200040, China
中国上海市延安西路65号上海国际贵都大饭店办公楼405单元
Phone: +86-21-62489820
Fax: +86-21-62489821

© 2011 The Author(s). Licensee IntechOpen. This is an open access article distributed under the terms of the [Creative Commons Attribution 3.0 License](https://creativecommons.org/licenses/by/3.0/), which permits unrestricted use, distribution, and reproduction in any medium, provided the original work is properly cited.

IntechOpen

IntechOpen